Radiology



# Diagnostic Accuracy of Intraocular Tumor Size Measured with MR Imaging in the Prediction of Postlaminar Optic Nerve Invasion and Massive Choroidal Invasion of Retinoblastoma[1]

Marcus C. De Jong, MD, MSc
Fenna J. S. van der Meer, MD
Sophia L. Göricke, MD
Hervé J. Brisse, MD, PhD
Paolo Galluzzi, MD
Philippe Maeder, MD
Selma Sirin, MD
Sonia De Francesco, MD
Xavier Sastre-Garau, MD, PhD
Klaus A. Metz, MD
Alfonso Cerase, MD
Daniel P. Noij, BSc
Paul van der Valk, MD, PhD
Annette C. Moll, MD, PhD
Jonas A. Castelijns, MD, PhD
Pim de Graaf, MD, PhD
For the European Retinoblastoma Imaging Collaboration

**Purpose:** To assess the correlation of intraocular retinoblastoma tumor size measured with magnetic resonance (MR) imaging in the prediction of histopathologically determined metastatic risk factors (postlaminar optic nerve invasion and massive choroidal invasion).

**Materials and Methods:** The ethics committee approved this retrospective multicenter study with a waiver of informed consent. The study population included 370 consecutive patients with retinoblastoma (375 eyes) who underwent baseline MR imaging, followed by primary enucleation from 1993 through 2014. Tumor sizes (maximum diameter and volume) were measured independently by two observers and correlated with histopathologic risk factors. Receiver operating characteristic curves were used to analyze the diagnostic accuracy of tumor size, and areas under the curve were calculated. Logistic regression analysis was performed to evaluate potential confounders.

**Results:** Receiver operating characteristic analysis of volume and diameter, respectively, yielded areas under the curve of 0.77 (95% confidence interval [CI]: 0.70, 0.85; $P < .0001$) and 0.78 (95% CI: 0.71, 0.85; $P < .0001$) for postlaminar optic nerve invasion ($n = 375$) and 0.67 (95% CI: 0.57, 0.77; $P = .0020$) and 0.70 (95% CI: 0.59, 0.80; $P = .0004$) for massive choroidal tumor invasion ($n = 219$). For the detection of cooccurring massive choroidal invasion and postlaminar optic nerve invasion ($n = 219$), volume and diameter showed areas under the curve of 0.81 (95% CI: 0.70, 0.91; $P = .0032$) and 0.83 (95% CI: 0.73, 0.93; $P = .0016$), respectively.

**Conclusion:** Intraocular tumor size shows a strong association with postlaminar optic nerve invasion and a moderate association with massive choroidal invasion. These findings provide diagnostic accuracy measures at different size cutoff levels, which could potentially be useful in a clinical setting, especially within the scope of the increasing use of eye-salvage treatment strategies.



*Online supplemental material is available for this article.*

[1] From the Departments of Radiology and Nuclear Medicine (M.C.d.J., F.J.S.v.d.M., D.P.N., J.A.C., P.d.G.), Pathology (P.v.d.V.), and Ophthalmology (A.C.M.), VU University Medical Center, PO Box 7057, 1007 MB Amsterdam, the Netherlands; Institute of Diagnostic and Interventional Radiology and Neuroradiology, University Hospital Essen, Germany (S.L.G., S.S.); Departments of Radiology (H.J.B.) and Tumor Biology (X.S.G.), Institut Curie, Paris, France; Unit of Neuroimaging and Neurointervention, Department of Neurosciences, Siena University Hospital, Siena, Italy (P.G., A.C.); Department of Radiology, Centre Hospitalier Universitaire Vaudois (CHUV) and University of Lausanne, Lausanne, Switzerland (P.M.); Unit of Ophthalmology, University of Siena, Policlinico Santa Maria alle Scotte, Siena, Italy (S.D.F.); and Department of Pathology and Neuropathology, Institute of Pathology and Neuropathology, Faculty of Medicine, University Duisburg-Essen, Essen, Germany (K.A.M.). Received June 1, 2015; revision requested August 7; revision received September 1; accepted October 5; final version accepted October 16. M.C.d.J. and the European Retinoblastoma Imaging Collaboration (ERIC) were supported by a grant from the ODAS Foundation, Delft, the Netherlands. The authors' work was independent of the funding organizations. The funding organizations had no involvement in the design or conduct of this study, data management and analysis, or manuscript preparation and review or authorization for submission. **Address correspondence to** M.C.d.J. (e-mail: *mc.dejong@vumc.nl*).

Retinoblastoma is a malignant tumor of the retina and represents approximately 3% of all pediatric malignancies (1). The incidence is one in every 17000 live births, with the retinoblastoma typically manifesting in the first 5 years of life (2). Retinoblastoma can be divided into two main groups: the hereditary form (about 40% of cases) and the nonhereditary form (60% of cases and always unilateral) (3).

Fundoscopy and ultrasonography (US) can be used to accurately stage intraocular retinoblastoma and distinguish it from other ocular lesions. To detect risk factors beyond what can be detected with fundoscopy and US, histopathologic analysis is required. Magnetic resonance (MR) imaging can be used to assess these risk factors, though not as reliably as histopathologic examination (4–7). Massive choroidal invasion (invasion of at least 3 mm in terms of thickness or width of the tumor into the choroid or touching the sclera [8]), scleral invasion, and postlaminar optic nerve invasion (PLONI) are considered metastatic risk factors (especially concomitant PLONI and massive choroidal or scleral invasion) (9–17). In the case of PLONI, the tumor has grown into the extraocular optic nerve posterior to the lamina cribrosa sclerae, a fibrous meshlike structure that divides the optic nerve into intraocular and extraocular parts.

Information about these risk factors is important when making the decision whether to enucleate or justify an eye-sparing treatment approach. Increasingly, patients with advanced retinoblastoma (International Classification of Retinoblastoma [ICRB] groups D and E [18,19]) are treated with eye-sparing treatment regimens (20,21), even patients with unilateral disease with no remaining vision in the affected eye (22). In a recent article by Ong et al (23), it was emphasized that accurate and early diagnosis of metastatic risk factors is essential. They showed that of 12 patients who were treated with intra-arterial chemotherapy, three developed central nervous system metastases, of whom two died; all three showed optic nerve and choroidal invasion (the exact degree of invasion into the optic nerve and choroid was not specified) when the eyes were (eventually) enucleated. Also, Zhao et al and Chantada et al showed the potential high risk of metastasis and death if proper treatment of advanced retinoblastoma is delayed (24,25).

Histopathologic examination is the reference standard for these risk factors. The diagnostic accuracy of MR imaging for the detection of metastatic risk factors is not perfect, but with the increasing use of eye-sparing treatment regimens, MR imaging is the only source of information to justify the choice of treatment (5,26). Previous, generally smaller studies have shown that there is an association between tumor size and tumor extent (26–29). We hypothesized that, in a larger sample size, we could show a clearer association between tumor size and tumor extent, allowing for clinically relevant risk modification.

The purpose of this study was to assess the correlation of the size of intraocular retinoblastoma measured with MR imaging in the prediction of histopathologically proven metastatic risk factors—that is, the tumor extent parameters of PLONI, massive choroidal invasion, and scleral invasion.

## Advances in Knowledge

- This study demonstrates a strong association between tumor size (volume and diameter) and postlaminar optic nerve invasion (PLONI, $P < .0001$).
- Intraocular tumor volume (≤0.88 $cm^3$ and >2.04 $cm^3$) shows potentially clinically useful likelihood ratios for the lack of PLONI (negative likelihood ratio, 0.08) and presence of PLONI (positive likelihood ratio, 6.35).
- The association between the presence of massive choroidal invasion and tumor volume ($P = .0020$) and tumor diameter ($P = .0004$) has not previously been well established in the literature.
- Tumor diameter and volume perform equally well in the prediction of PLONI and massive choroidal invasion.

## Implications for Patient Care

- Improved detection of metastatic risk factors of retinoblastoma helps in choosing the most appropriate treatment regimen, especially as the use of eye-salvage treatment strategies increases.
- Physicians should be aware that even in eyes with small intraocular tumors (≥0.19 $cm^3$ or 8.15 mm), there is a risk of massive choroidal invasion.
- Concomitant PLONI and massive choroidal invasion occurred only in relatively large tumors (≥1.40 $cm^3$ or 16.50 mm).

## Materials and Methods

We performed this study according to the Standards for Reporting of Diagnostic Accuracy statement (30).

**Published online before print**
10.1148/radiol.2015151213 **Content codes:** HN MR

**Radiology 2016;** 279:817–826

**Abbreviations:**
AUC = area under the curve
CI = confidence interval
ICC = intraclass correlation coefficient
ICRB = International Classification of Retinoblastoma
IQR = interquartile range
PLONI = postlaminar optic nerve invasion
ROC = receiver operating characteristic
ROI = region of interest

**Author contributions:**
Guarantors of integrity of entire study, M.C.d.J., S.D.F., J.A.C., P.d.G.; study concepts/study design or data acquisition or data analysis/interpretation, all authors; manuscript drafting or manuscript revision for important intellectual content, all authors; approval of final version of submitted manuscript, all authors; agrees to ensure any questions related to the work are appropriately resolved, all authors; literature research, M.C.d.J., P.M., K.A.M., A.C., D.P.N., P.v.d.V., J.A.C.; clinical studies, H.J.B., P.G., P.M., S.S., S.D.F., K.A.M., J.A.C., P.d.G.; experimental studies, K.A.M., P.v.d.V., J.A.C.; statistical analysis, M.C.d.J., K.A.M., J.A.C.; and manuscript editing, M.C.d.J., S.L.G., P.G., P.M., S.S., K.A.M., A.C., D.P.N., P.v.d.V., A.C.M., J.A.C., P.d.G.

Conflicts of interest are listed at the end of this article.

### Patient Population

Eligible patients were retrospectively selected from a consecutive series of patients with retinoblastoma from four European Retinoblastoma Imaging Collaboration centers. Inclusion criteria for this study were as follows. *(a)* The patient received a diagnosis of retinoblastoma. *(b)* Baseline MR images were available, including T1-weighted contrast material–enhanced images with a section thickness less than 4 mm. *(c)* The patient underwent primary enucleation of the affected eye(s) (ie, no previous treatment was administered for retinoblastoma, and there were no more than 14 days between baseline imaging and enucleation). *(d)* Adequate histopathologic results were available. Inclusion criteria were met by 154 patients from Amsterdam, the Netherlands (from January 1993 through December 2013; exclusions were based on criteria *b* [$n$ = 13], *c* [$n$ = 83], and *d* [$n$ = 6]), 51 patients from Paris, France (from July 2006 through January 2014; exclusions were based on criteria *b* [$n$ = 129] and *c* [$n$ = 255]), 137 patients from Essen, Germany (from January 2007 through June 2012; exclusions were based on criterion *c* [$n$ = 163]), and 28 patients from Siena, Italy (from June 2009 through January 2014; exclusions were based on criterion *c* [$n$ = 171]). From the four centers, we included a total of 370 patients and 375 eyes (five patients underwent bilateral primary enucleation). We assumed independence in case two eyes from one patient were included. The ethics committee approved this retrospective study, with a waiver of informed consent.

Histopathologic data (there was no central pathology review; histopathologic analysis was performed by local neuropathologists, including P.v.d.V., K.A.M., and X.S.G., with 15, 31, and 25 years of experience, respectively) and clinical data (including the ICRB groups [18,19]) were extracted from medical records. Eyes without an ICRB score were retrospectively scored by A.C.M. (with 25 years of experience in retinoblastoma ophthalmology) on the basis of clinical data from medical records, blinded for histopathologic and radiologic data. Histopathologic data from Amsterdam, the Netherlands (dating further back than the other centers), were incomplete for massive choroidal and scleral invasion and were therefore excluded from analyses of these parameters. Included data partially overlap with data used for tumor volume analysis in studies by De Graaf et al (29) and Brisse et al (26).

### Imaging Protocols

The MR imaging units used included a 1.0-T system (Magnetom Impact Expert; Siemens, Erlangen, Germany; head coil, $n$ = 20), 1.5-T systems (Magnetom Vision, Sonata, Symphony, Avanto, or Aera; Siemens; head coil, $n$ = 57; and surface coil, $n$ = 284), and a 3-T system (Discovery MR750; GE Healthcare, Little Chalfont, United Kingdom; head coil, $n$ = 9). A wide range of different imaging protocols was used. The section thickness ranged from 1.5 to 3.0 mm, the intersection gap ranged from 0.0 to 0.4 mm, and the median pixel size was 0.27 × 0.27 $mm^2$ (range, 0.15 × 0.15 to 0.98 × 0.98 $mm^2$). To test the effect of image resolution on the results, we performed subgroup analysis by only including high-spatial-resolution images—that is, the resolution should be at least 0.5 × 0.5 × 2.0 $mm^3$ (with pixel dimension on the x- and y-axes and section thickness on the z-axis); this minimum resolution was recommended by De Graaf et al (4) in the guidelines they published on retinoblastoma imaging.

### Tumor Diameter and Volume Measurement

Two observers who were blinded to clinical and histopathologic data (P.d.G. and M.C.d.J., with 12 and 2 years of experience in ocular MR imaging, respectively) used a picture archiving and communication system (Sectra, Linköping, Sweden) to independently draw regions of interest (ROIs) on every section that contained tumor mass. All images were originally digitally stored. Both T2-weighted images and contrast-enhanced T1-weighted images were used to distinguish tumor mass from nontumor mass. The ROIs were drawn on contrast-enhanced T1-weighted images. Volumes were calculated by summing up the surface areas multiplied by the section thickness, plus intersection gap. The two observers also independently extracted maximum tumor diameter (ie, the largest continuous line through the tumor mass on axial images; in the case of multiple tumor masses, the diameter of the largest mass was determined; when axial images were missing, sagittal images were used) and distance of the tumor to the optic nerve (≥2 mm from the optic disk, <2 mm from the optic disk, or totally or partially covering the optic disk).

For statistical analysis, we combined the results from the two readers by calculating mean volumes and diameters when the difference between the two readers was up to 5% for volume and up to 1 mm for diameter. In case the difference between the two readers was more than that, consensus volumes or diameters were determined by performing measurements together. Discrepancies were solved by means of consensus.

### Statistical Analysis

Interobserver agreement (intraclass correlation coefficient [ICC] for volume and diameter) and the Cohen κ coefficient for the distance of the tumor to the optic disk were calculated on the basis of preconsensus data. We used receiver operating characteristic (ROC) analysis to determine the area under the curve (AUC) to assess the diagnostic accuracy of tumor volume and diameter in the prediction of tumor extent (invasion into the choroid and optic nerve).

We included diagnostic accuracy measures of optimal cutoff values on the basis of ROC analysis by maximizing the Youden index (Youden index = sensitivity + specificity − 1) in the upper, intermediate, and lower tumor size ranges (31). We selected a lower cutoff value in the range where sensitivity did not fall below 90%, and we selected the upper cutoff value in the range where specificity did not fall below 90%; the

intermediate cutoff value was determined in the range where sensitivity and specificity were both less than 90%.

To evaluate potential confounders, we performed logistic regression analysis. Potentially confounding variables were verified in univariable analysis first. When such a variable was identified as being statistically significant ($P < .05$), it was included in a multivariable logistic regression model with tumor volume and diameter. Because of the relatively low number of events, we chose to limit the number of variables in the multivariable analysis (32). For statistical analyses, we used SPSS software version 20 (IBM, Armonk, NY).

## Results

The included patients ($n$ = 370) had a median age of 20 months (interquartile range [IQR], 10–31 months); 203 (55%) were male, and 98 (26%) had bilateral retinoblastoma. The median time between baseline MR imaging and enucleation was 5 days (IQR, 2–7 days; range, 0–14 days). The ICRB scores of the included eyes ($n$ = 375) were zero group A eyes, eight group B eyes (2%), seven group C eyes (2%), 127 group D eyes (34%), and 233 group E eyes (62%). Figure 1 depicts how we placed the ROIs and diameters on MR images.

### Interobserver Agreement

The median volumes were 1.17 $cm^3$ (IQR, 0.74–1.62 $cm^3$) and 1.16 $cm^3$ (IQR, 0.74–1.64, $cm^3$), respectively, as measured by observers 1 and 2. Median diameters were 15.10 mm (IQR, 13.30–17.20 mm) and 15.40 mm (IQR, 13.20–17.20 mm), respectively. The preconsensus measurements gave an excellent ICC of 0.98 for volume (95% confidence interval [CI]: 0.98, 0.99) and a good ICC of 0.92 for diameter (95% CI: 0.90, 0.93). Distance of the tumor to the optic disk (Table E1 [online]) shows reasonably good agreement between the two observers (κ = 0.71; 95% CI: 0.60, 0.82).

High-spatial-resolution images ($n$ = 294; voxel size ≤ 0.5 × 0.5 × 2.0 $mm^3$) showed ICCs of 0.99 (95% CI: 0.98, 0.99) for volume and 0.93 (95% CI: 0.91, 0.94) for diameter, and the κ value for distance to the optic disk increased to 0.76 (95% CI: 0.63, 0.89). Low-resolution images ($n$ = 81) yielded ICCs of 0.95 (95% CI: 0.93, 0.97) and 0.87 (95% CI: 0.81, 0.92) and a κ value of 0.61 (95% CI: 0.41, 0.83).

**Figure 1**

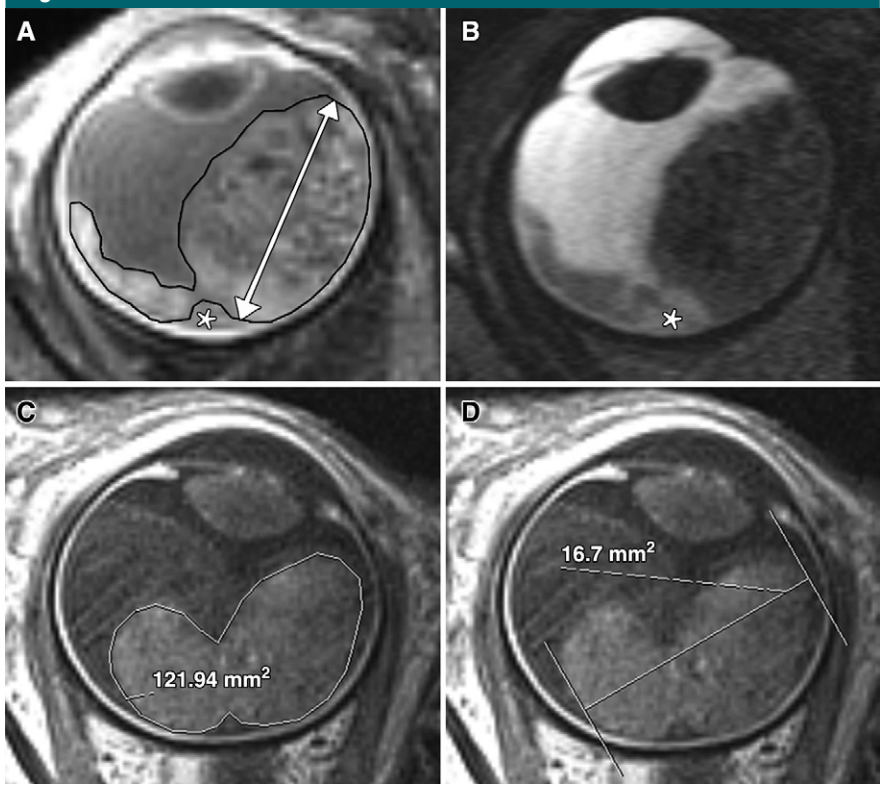


**Figure 1:** Axial MR images show tumor volume and diameter determination. *A,* Schematic representation of maximum diameter (white line) and tumor surface (black contour) determination is shown on a contrast-enhanced T1-weighted MR image, with the help of, *B,* a T2-weighted MR image. The asterisk on *A* represents a contrast-enhancing area that could be classified as subretinal fluid on image *B* (a high-intensity area compared with the low-intensity area that represents the tumor) and could therefore be excluded from the ROI. *C,* Image shows the actual determination of volume (tumor surface × [section thickness + intersection gap]). *D,* Image shows the actual determination of the diameter on a contrast-enhanced T1-weighted MR image in the picture archiving and communication system.

### Analysis of Tumor Volume, Diameter, and Location

Median consensus volume and diameter were 1.17 $cm^3$ (IQR, 0.75–1.65 $cm^3$) and 15.37 mm (IQR, 13.40–17.30 mm), respectively, for all included eyes. Table 1 depicts tumor sizes for each tumor extent parameter. Tumor sizes differed significantly for PLONI (37 of 375 eyes) and massive choroidal invasion (33 of 219 eyes) (Figure E1 [online]). When the tumor appears separate from the optic disk on MR images, there is still a risk of optic nerve invasion, but in all cases of PLONI, the tumor also touched the optic nerve (Table E1 [online]). All eyes with PLONI had a tumor volume of at least 0.59 $cm^3$ and a diameter of at least 13.90 mm, and eyes with massive choroidal invasion showed a tumor volume of at least 0.19 $cm^3$ and a diameter of at least 8.15 mm, whereas we only found concomitant PLONI and massive choroidal invasion in eyes with a tumor volume of at least 1.40 $cm^3$ and a diameter of at least 16.50 mm.

**Table 1**

**Tumor Volumes and Diameters**

| Finding and Presence at Histopathologic Examination | No. of Eyes | Prevalence (%) | Percentage Touching the Optic Disk on MR Images (%) | Median Tumor Volume | | Median Tumor Diameter | |
|---|---|---|---|---|---|---|---|
| | | | | Measurement ($cm^3$) | *P* Value | Measurement (mm) | *P* Value |
| Optic nerve invasion | | | | | <.0001 | | <.0001 |
| No | 167 | 45 | 77.2 | 0.94 (0.62–1.39) | | 14.30 (12.30–16.35) | |
| Yes | 208 | 55 | 94.7 | 1.37 (0.94–1.76) | | 16.18 (14.21–18.00) | |
| Postlaminar invasion | | | | | <.0001 | | <.0001 |
| No | 338 | 90 | 85.5 | 1.12 (0.71–1.58) | | 15.10 (13.07–16.90) | |
| Yes | 37 | 10 | 100.0 | 1.70 (1.37–2.28) | | 17.92 (15.85–19.28) | |
| Choroidal invasion | | | | | .0002 | | .0016 |
| No | 273 | 73 | … | 1.09 (0.70–1.52) | | 15.10 (13.08–16.95) | |
| Yes | 102 | 27 | … | 1.41 (0.94–1.85) | | 16.54 (13.99–18.06) | |
| Massive choroidal invasion* | | | | | .0020 | | .0004 |
| No | 186 | 85 | … | 1.19 (0.73–1.67) | | 15.44 (13.41–17.41) | |
| Yes | 33 | 15 | … | 1.58 (1.21–2.08) | | 17.40 (15.38–19.43) | |
| Scleral invasion* | | | | | .12 | | .24 |
| No | 214 | 98 | … | 1.27 (0.77–1.70) | | 15.83 (13.65–17.65) | |
| Yes | 5 | 2 | … | 2.42 (0.80–2.65) | | 18.50 (12.33–19.37) | |
| Postlaminar invasion or massive choroidal invasion*† | | | | | <.0001 | | <.0001 |
| No | 174 | 79 | … | 1.13 (0.68–1.62) | | 15.15 (13.11–17.00) | |
| Yes | 45 | 21 | … | 1.66 (1.36–2.13) | | 17.92 (16.68–19.45) | |
| Postlaminar invasion and massive choroidal invasion*† | | | | | .0032 | | .0016 |
| No | 211 | 96 | … | 1.25 (0.76–1.69) | | 15.65 (13.55–17.50) | |
| Yes | 8 | 4 | … | 2.08 (1.46–2.15) | | 18.21 (17.34–20.44) | |

Note.—Numbers in parentheses are IQRs. *P* values for the differences in volume and diameter per tumor extent variable were obtained with the Mann-Whitney *U* test (two sided).

* Excluding Amsterdam data.

† Eight eyes had concomitant PLONI and massive choroidal invasion, 25 had only massive choroidal invasion, and 12 had only PLONI.

## ROC Analysis

The ROC analysis for tumor volume and diameter, respectively, yielded AUCs of 0.67 (95% CI: 0.62, 0.73; $P < .0001$) and 0.68 (95% CI: 0.63, 0.73; $P < .0001$) for any optic nerve invasion ($n = 375$, 208 events) and AUCs of 0.77 (95% CI: 0.70, 0.85; $P < .0001$) and 0.78 (95% CI: 0.71, 0.85; $P < .0001$) for PLONI ($n = 375$, 37 events; Fig 2a).

Similar analyses yielded AUCs of 0.63 (95% CI: 0.56, 0.69; $P = .0002$) and 0.61 (95% CI: 0.54, 0.67; $P = .0016$) for choroidal invasion ($n = 375$, 102 events) and AUCs of 0.67 (95% CI: 0.57, 0.77; $P = .0020$) and 0.70 (95% CI: 0.59, 0.80; $P = .0004$) for massive choroidal invasion ($n = 219$, 33 events; Fig 2c), respectively. Scleral invasion ($n = 219$, five events) was only present in five eyes and yielded AUCs of 0.71 (95% CI: 0.38, 1.00; $P = .11$) and 0.66 (95% CI: 0.35, 0.96; $P = .23$), respectively, for volume and diameter (Fig 2d).

Repeating the ROC calculations with only high-spatial-resolution images resulted in the exclusion of 81 of 375 eyes from the analysis of PLONI and three of 219 eyes from the analysis of massive choroidal invasion. For PLONI ($n = 294$, 32 events), this resulted in AUCs of 0.81 (95% CI: 0.74, 0.88; $P < .0001$) and 0.82 (95% CI: 0.75, 0.88; $P < .0001$), respectively, for volume and diameter (Fig 2b). The results for massive choroidal invasion did not change.

When we looked at either massive choroidal invasion or PLONI ($n = 219$, 45 events), volume yielded an AUC of 0.74 (95% CI: 0.66, 0.82; $P < .0001$), and diameter yielded an AUC of 0.77 (95% CI: 0.69, 0.85; $P < .0001$; Fig 2e). For cases with both massive choroidal invasion and PLONI ($n = 219$, eight events), volume yielded an AUC of 0.81 (95% CI: 0.70, 0.91; $P = .0032$), and diameter yielded an AUC of 0.83 (95% CI: 0.73, 0.93; $P = .0016$; Fig 2f).

Tables 2–4 summarize the different diagnostic accuracy measures of volume and diameter for the prediction of PLONI and massive choroidal invasion at different optimal cutoff levels based on maximization of the Youden index in the respective ROC curves.

## Tumor Size Compared with Optic Nerve Contrast Enhancement

In 23% of all cases (87 of 375, all with high-spatial-resolution images), we also had data on contrast enhancement (in millimeters posterior to the lamina

**Figure 2**

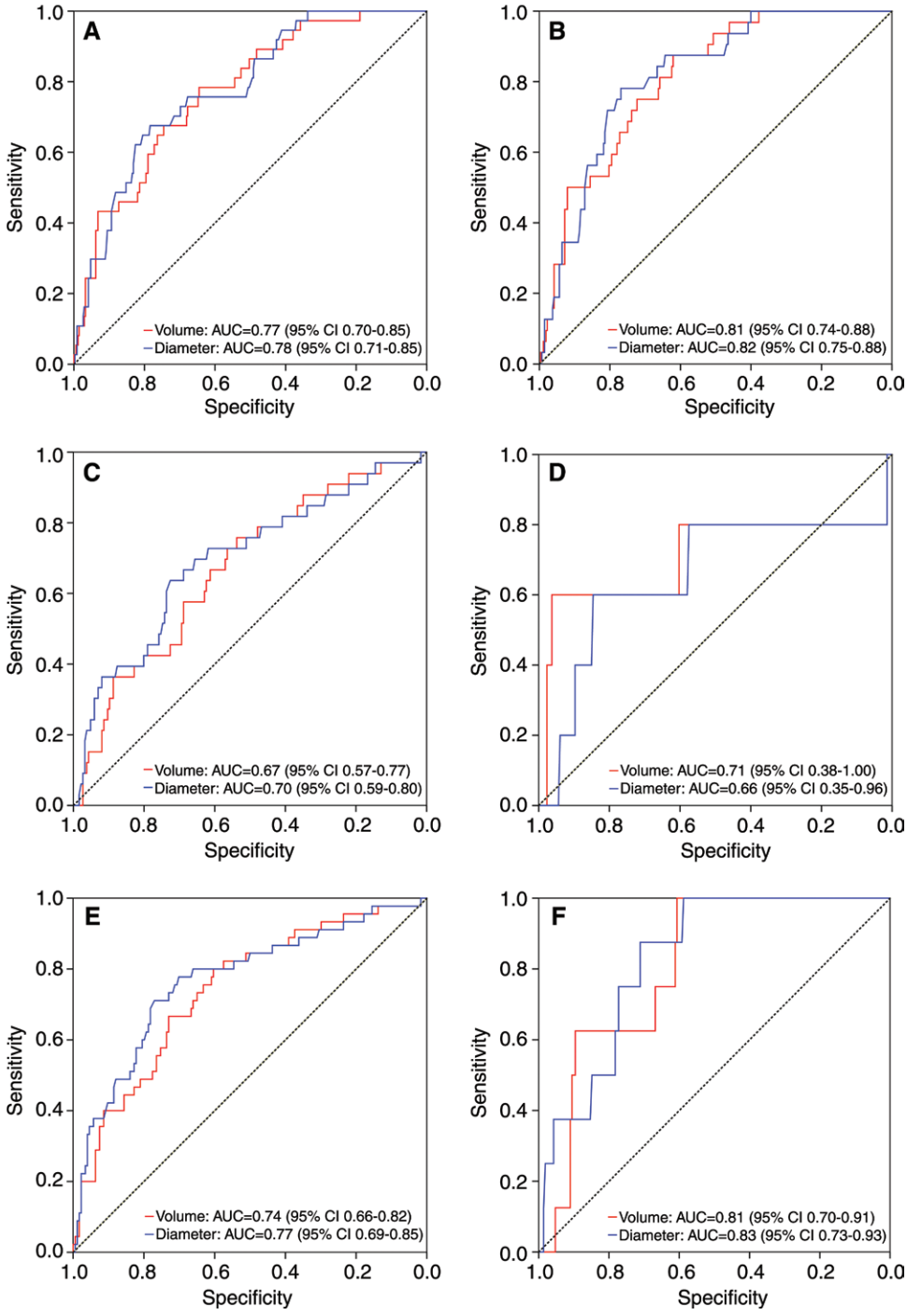


**Figure 2:** ROC curves of tumor volume (red) and diameter (blue) for, *A,* PLONI ($n = 375$, 37 events), *B,* high-spatial-resolution PLONI images only ($n = 294$, 32 events), *C,* massive choroidal invasion ($n = 219$, 33 events), *D,* scleral invasion ($n = 219$, five events), *E,* either postlaminar optic nerve or massive choroidal invasion ($n = 219$, 45 events), and, *F,* both postlaminar optic nerve and massive choroidal invasion ($n = 219$, eight events).

**Table 2**

**Diagnostic Accuracy of Tumor Size at Different Cutoff Levels in the Prediction of PLONI**

| Parameter | TP | FN | FP | TN | Sensitivity | Specificity | Positive Likelihood Ratio | Negative Likelihood Ratio | Youden Index |
|---|---|---|---|---|---|---|---|---|---|
| Volume ($cm^3$) | | | | | | | | | |
| 0.88* | 36 | 1 | 217 | 121 | 0.97 (0.86, 1.00) | 0.36 (0.31, 0.41) | 1.52 (1.24, 1.70) | 0.08 (0.00, 0.46) | 0.33 |
| 1.36† | 29 | 8 | 121 | 217 | 0.78 (0.62, 0.90) | 0.64 (0.59, 0.69) | 2.19 (1.50, 2.94) | 0.34 (0.14, 0.65) | 0.43 |
| 2.04‡ | 16 | 21 | 23 | 315 | 0.43 (0.27, 0.61) | 0.93 (0.90, 0.96) | 6.35 (2.70, 13.87) | 0.61 (0.41, 0.81) | 0.36 |
| 1.15*§ | 30 | 2 | 131 | 131 | 0.94 (0.79, 0.99) | 0.51 (0.45, 0.57) | 1.90 (1.43, 2.31) | 0.12 (0.01, 0.47) | 0.45 |
| 1.36†§ | 28 | 4 | 100 | 162 | 0.88 (0.71, 0.96) | 0.62 (0.56, 0.68) | 2.29 (1.60, 2.99) | 0.20 (0.05, 0.52) | 0.49 |
| 2.04‡§ | 16 | 16 | 20 | 242 | 0.50 (0.32, 0.68) | 0.92 (0.88, 0.95) | 6.55 (2.76, 14.42) | 0.54 (0.33, 0.77) | 0.42 |
| Diameter (mm) | | | | | | | | | |
| 14.4* | 35 | 2 | 199 | 139 | 0.95 (0.82, 0.99) | 0.41 (0.36, 0.47) | 1.61 (1.27, 1.86) | 0.13 (0.01, 0.51) | 0.36 |
| 17.2† | 25 | 12 | 73 | 265 | 0.68 (0.50, 0.82) | 0.78 (0.74, 0.83) | 3.13 (1.90, 4.73) | 0.41 (0.22, 0.68) | 0.46 |
| 18.5‡ | 14 | 23 | 32 | 306 | 0.38 (0.22, 0.55) | 0.91 (0.87, 0.93) | 4.00 (1.71, 8.41) | 0.69 (0.48, 0.89) | 0.28 |
| 15.0*§ | 30 | 2 | 140 | 122 | 0.94 (0.79, 0.99) | 0.47 (0.40, 0.53) | 1.75 (1.33, 2.10) | 0.13 (0.01, 0.51) | 0.40 |
| 17.2†§ | 25 | 7 | 60 | 202 | 0.78 (0.60, 0.91) | 0.77 (0.72, 0.82) | 3.41 (2.11, 5.05) | 0.28 (0.11, 0.56) | 0.55 |
| 19.2‡§ | 11 | 21 | 16 | 246 | 0.34 (0.19, 0.53) | 0.94 (0.90, 0.96) | 5.63 (1.91, 15.07) | 0.70 (0.49, 0.90) | 0.28 |

Note.—Numbers in parentheses are 95% CIs. FN = false-negative findings, FP = false-positive findings, TN = true-negative findings, TP = true-positive findings.

* The highest Youden index was achieved with a sensitivity ≥ 0.90.

† Highest overall Youden index.

‡ The highest Youden index was achieved with a specificity ≥ 0.90.

§ Only high-spatial-resolution MR imaging was used (pixel size ≤ 0.5 × 0.5 $mm^2$ and section thickness ≤ 2.0 mm).

**Table 3**

**Diagnostic Accuracy of Tumor Size at Different Size Cutoff Levels in the Prediction of Massive Choroidal Invasion**

| Parameter | TP | FN | FP | TN | Sensitivity | Specificity | Positive Likelihood Ratio | Negative Likelihood Ratio | Youden Index |
|---|---|---|---|---|---|---|---|---|---|
| Volume ($cm^3$) | | | | | | | | | |
| 0.78* | 30 | 3 | 134 | 52 | 0.91 (0.76, 0.98) | 0.28 (0.22, 0.35) | 1.26 (0.97, 1.51) | 0.33 (0.05, 1.12) | 0.19 |
| 1.27† | 25 | 8 | 86 | 100 | 0.76 (0.58, 0.89) | 0.54 (0.46, 0.61) | 1.64 (1.08, 2.28) | 0.45 (0.18, 0.91) | 0.30 |
| 2.06‡ | 9 | 24 | 18 | 168 | 0.27 (0.13, 0.46) | 0.90 (0.85, 0.94) | 2.82 (0.89, 7.80) | 0.81 (0.58, 1.02) | 0.18 |
| Diameter (mm) | | | | | | | | | |
| 13.0* | 30 | 3 | 145 | 41 | 0.91 (0.76, 0.98) | 0.22 (0.16, 0.29) | 1.17 (0.90, 1.38) | 0.41 (0.07, 1.49) | 0.13 |
| 17.1† | 21 | 12 | 51 | 135 | 0.64 (0.45, 0.80) | 0.73 (0.66, 0.79) | 2.32 (1.31, 3.76) | 0.50 (0.26, 0.84) | 0.36 |
| 18.9‡ | 12 | 21 | 15 | 171 | 0.36 (0.20, 0.55) | 0.92 (0.87, 0.95) | 4.51 (1.58, 11.97) | 0.69 (0.47, 0.91) | 0.28 |

Note.—Numbers in parentheses are 95% CIs. FN = false-negative findings, FP = false-positive findings, TN = true-negative findings, TP = true-positive findings.

* The highest Youden index was achieved with a sensitivity ≥ 0.90.

† Highest overall Youden index.

‡ The highest Youden index was achieved with a specificity ≥ 0.90.

cribrosa); this was published before in an article by Brisse et al (26). Figure 3 shows the distribution of eyes with (red circles) and without (green circles) histopathologically proven PLONI for tumor volume (y-axis) versus optic nerve contrast enhancement on T1-weighted images (x-axis). Of nine cases of PLONI, five showed no contrast enhancement, whereas 12 of 87 cases without PLONI did show enhancement.

### Logistic Regression Analysis

For massive choroidal invasion ($n$ = 219) and PLONI ($n$ = 375), age at baseline imaging, disease laterality, patient sex, and multicenter location (referral center) were all statistically insignificant ($P$ ≥ .05) in univariable analysis and had low estimates of goodness of fit (Table E2 [online]). Also, adding these variables to a multivariable model hardly influenced the estimates for volume and diameter from univariable analysis (data not shown). The ICRB score (likely not independent from tumor size) did have a significant effect ($P$ = .036) as a univariable predictor of PLONI. However, ICRB score was insignificant in a multivariable model with volume or diameter. Also, the goodness of fit values show that volume and diameter explain the presence of PLONI much better than any other variable; to a lesser extent,

**Table 4**

**Diagnostic Accuracy of Tumor Size at Different Size Cutoff Levels in the Prediction of Concomitant PLONI and Massive Choroidal Invasion**

| Parameter | TP | FN | FP | TN | Sensitivity | Specificity | Positive Likelihood Ratio | Negative Likelihood Ratio | Youden Index |
|---|---|---|---|---|---|---|---|---|---|
| Volume ($cm^3$) | | | | | | | | | |
| 1.40*† | 8 | 0 | 83 | 128 | 1.00 (0.63, 1.00) | 0.61 (0.54, 0.67) | 2.54 (1.36, 3.06) | 0.00 (0.00, 0.69) | 0.61 |
| 2.06‡ | 5 | 3 | 22 | 189 | 0.63 (0.24, 0.91) | 0.90 (0.85, 0.93) | 5.99 (1.59, 13.75) | 0.42 (0.09, 0.89) | 0.52 |
| Diameter (mm) | | | | | | | | | |
| 16.5*† | 8 | 0 | 87 | 124 | 1.00 (0.63, 1.00) | 0.59 (0.52, 0.65) | 2.43 (1.31, 2.90) | 0.00 (0.00, 0.71) | 0.59 |
| 19.6‡ | 3 | 5 | 9 | 202 | 0.38 (0.09, 0.76) | 0.96 (0.92, 0.98) | 8.79 (1.07, 38.36) | 0.65 (0.25, 0.99) | 0.33 |

Note.—Numbers in parentheses are 95% CIs. FN = false-negative findings, FP = false-positive findings, TN = true-negative findings, TP = true-positive findings.

* The highest Youden index was achieved with a sensitivity ≥ 0.90.

† Highest overall Youden index.

‡ The highest Youden index was achieved with a specificity ≥ 0.90.

**Figure 3**

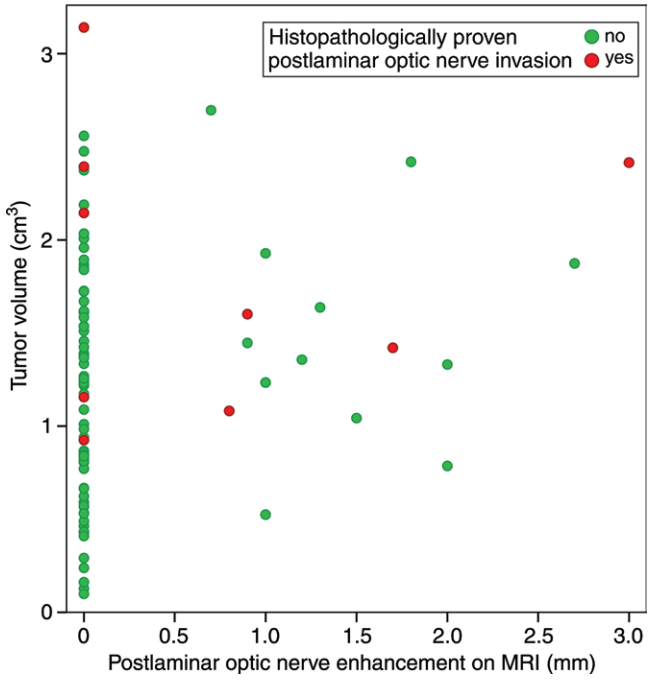


**Figure 3:** Plot of tumor volume (in cubic centimeters) versus postlaminar optic nerve enhancement (in millimeters) on T1-weighted MR images for eyes with ($n$ = 9) and those without ($n$ = 78) PLONI.

this also applies to massive choroidal invasion. See Table E2 (online) for the logistic regression results.

## Discussion

In the current study, we demonstrated that both PLONI and massive choroidal invasion were significantly associated with intraocular retinoblastoma tumor size. Tumor size showed a reasonably good diagnostic accuracy in the prediction of PLONI and limited diagnostic accuracy in the prediction of massive choroidal invasion. Where PLONI was only seen in eyes with relatively large tumors, there remained a considerable risk of massive choroidal invasion in eyes with small tumors. Also, concomitant massive choroidal invasion and PLONI—for which there is evidence of increased risk of metastatic disease (11)—was only found in large tumors in our study. Scleral invasion is probably also associated with tumor size, but the number of patients with scleral invasion was too low to show a significant difference in tumor size. In cases where the tumor seems to be separate from the optic disk on MR images, there is still a risk of prelaminar optic nerve invasion, but we did not find any postlaminar invasion in tumors that appeared separate from the optic disk. This phenomenon could be explained by the presence of (vitreous) tumor seeds on the optic disk, which can lead to invasive growth into the optic nerve (29).

Two previously published studies (with a population that did not overlap with this study) showed a statistically significant association between PLONI and tumor diameter (27,28), which was confirmed in the current study. Yan and colleagues (28) showed a significant association between scleral invasion and tumor diameter and thickness. Furthermore, our study showed a significant association between tumor volume and PLONI, as well, and a significant association between massive choroidal invasion and both tumor volume and diameter, which has not previously been well established in the literature.

Compared with older studies, the large sample size of our study allowed

us to construct clinically applicable tumor size cutoff levels. These cutoff levels might assist physicians in determining posttest risk profiles to (for example) help decide *(a)* when the risk of PLONI or massive choroidal invasion is low enough to justify an eye-sparing treatment strategy (which is especially important in a time when selective intra-arterial chemotherapy is increasingly used as a first-line treatment for advanced-stage retinoblastoma [21,33]) or *(b)* when the risk is too high for eye-sparing treatment, in which case enucleation can be performed and—after histopathologic results are available—preventive adjuvant systemic chemotherapy can be chosen.

Logistic regression analysis shows that PLONI is best predicted according to tumor size and much less with the other tested variables. Other than tumor size, ICRB score (group D or lower vs group E) was the only parameter that allowed significant prediction of PLONI in univariable analysis, which is in line with findings from Kaliki et al (16) and Yan et al (28). However, in multivariable analysis, the effect of ICRB score diminished. Logistic regression analysis also shows that tumor size is the only significant predictor of massive choroidal invasion, but, as expected, the predictive value is lower than that for PLONI. We included patients from four retinoblastoma referral centers, each with different criteria for enucleation (eg, patients from one center might have more advanced retinoblastoma than patients from another center). However, logistic regression analysis did not show a significant influence of multicenter location on the results.

This study does have some limitations. A potential bias might be that we could only include patients who underwent enucleation, as histopathologic results were only available for this group. Thus, by definition, all included patients had advanced retinoblastoma. To what extent the results of this study are also valid for less advanced disease is hard to say, but if a bias has been introduced, it is because patients with small tumors and without other risk factors of metastatic disease were not included. The risk of PLONI and massive choroidal invasion may well be lower for less advanced retinoblastoma, not only because the tumor sizes are generally smaller, but also because of other prognostic factors (eg, perhaps the tumors are less aggressive). Histopathologic analysis was performed by experienced pathologists, but unfortunately, we were not able to perform central pathology review. When compared with tumor volume, tumor diameter might be not as accurate in the case of multiple lesions or complex shapes, as we defined diameter as the largest "uninterrupted" diameter through the tumor. Nevertheless, this did not influence diagnostic accuracy negatively, because both tumor diameter and volume showed comparable results.

In conclusion, intraocular tumor size is strongly associated with PLONI and moderately associated with massive choroidal invasion. Tumor diameter and volume both performed similarly, but volume can be obtained more reliably. This article provides diagnostic accuracy measures at different size cutoff levels that will potentially be useful in a clinical setting, especially within the scope of a strong increase in eye-salvage treatment strategies.

**The European Retinoblastoma Imaging Collaboration is as follows:** Jonas A. Castelijns, MD, PhD, Pim de Graaf, MD, PhD, and Marcus C. de Jong, MD, MSc, at the Department of Radiology and Nuclear Medicine, VU University Medical Center, Amsterdam, the Netherlands; Hervé J. Brisse, MD, PhD, at the Department of Radiology, Institut Curie, Paris, France; Paolo Galluzzi, MD, at the Unit of Diagnostic and Therapeutic Neuroradiology, Department of Neurosciences, Siena University Hospital, Siena, Italy; Sophia Göricke, MD, and Selma Sirin, MD, at the Institute of Diagnostic and Interventional Radiology and Neuroradiology, University Hospital Essen, Essen, Germany; and Philippe Maeder, MD, at the Department of Radiology, Centre Hospitalier Universitaire Vaudois (CHUV), and the University of Lausanne, Lausanne, Switzerland.

**Disclosures of Conflicts of Interest: M.C.d.J.** disclosed no relevant relationships. **F.J.S.v.d.M.** disclosed no relevant relationships. **S.L.G.** disclosed no relevant relationships. **H.J.B.** disclosed no relevant relationships. **P.G.** disclosed no relevant relationships. **P.M.** disclosed no relevant relationships. **S.S.** disclosed no relevant relationships. **S.D.F.** disclosed no relevant relationships. **X.S.G.** disclosed no relevant relationships. **K.A.M.** disclosed no relevant relationships. **A.C.** disclosed no relevant relationships. **D.P.N.** disclosed no relevant relationships. **P.v.d.V.** disclosed no relevant relationships. **A.C.M.** disclosed no relevant relationships. **J.A.C.** disclosed no relevant relationships. **P.d.G.** disclosed no relevant relationships.

## References

1. Rodriguez-Galindo C, Orbach DB, VanderVeen D. Retinoblastoma. Pediatr Clin North Am 2015;62(1):201–223.
2. Moll AC, Kuik DJ, Bouter LM, et al. Incidence and survival of retinoblastoma in the Netherlands: a register-based study 1862–1995. Br J Ophthalmol 1997;81(7):559–562.
3. Marees T, van Leeuwen FE, de Boer MR, Imhof SM, Ringens PJ, Moll AC. Cancer mortality in long-term survivors of retinoblastoma. Eur J Cancer 2009;45(18):3245–3253.
4. de Graaf P, Göricke S, Rodjan F, et al. Guidelines for imaging retinoblastoma: imaging principles and MRI standardization. Pediatr Radiol 2012;42(1):2–14.
5. de Jong MC, de Graaf P, Noij DP, et al. Diagnostic performance of magnetic resonance imaging and computed tomography for advanced retinoblastoma: a systematic review and meta-analysis. Ophthalmology 2014;121(5):1109–1118.
6. de Jong MC, de Graaf P, Brisse HJ, et al. The potential of 3T high-resolution magnetic resonance imaging for diagnosis, staging, and follow-up of retinoblastoma. Surv Ophthalmol 2015;60(4):346–355.
7. de Graaf P, Moll AC, Imhof SM, van der Valk P, Castelijns JA. Retinoblastoma and optic nerve enhancement on MRI: not always extraocular tumour extension. Br J Ophthalmol 2006;90(6):800–801.
8. Sastre X, Chantada GL, Doz F, et al. Proceedings of the consensus meetings from the International Retinoblastoma Staging Working Group on the pathology guidelines for the examination of enucleated eyes and evaluation of prognostic risk factors in retinoblastoma. Arch Pathol Lab Med 2009;133(8):1199–1202.
9. Shields CL, Shields JA, Baez KA, Cater J, De Potter PV. Choroidal invasion of retinoblastoma: metastatic potential and clinical risk factors. Br J Ophthalmol 1993;77(9):544–548.
10. Shields CL, Shields JA, Baez K, Cater JR, De Potter P. Optic nerve invasion of retinoblastoma. Metastatic potential and clinical risk factors. Cancer 1994;73(3):692–698.

11. Chantada GL, Casco F, Fandiño AC, et al. Outcome of patients with retinoblastoma and postlaminar optic nerve invasion. Ophthalmology 2007;114(11):2083–2089.

12. Chantada GL, Dunkel IJ, Antoneli CBG, et al. Risk factors for extraocular relapse following enucleation after failure of chemoreduction in retinoblastoma. Pediatr Blood Cancer 2007;49(3):256–260.

13. Uusitalo MS, Van Quill KR, Scott IU, Matthay KK, Murray TG, O'Brien JM. Evaluation of chemoprophylaxis in patients with unilateral retinoblastoma with high-risk features on histopathologic examination. Arch Ophthalmol 2001;119(1):41–48.

14. Honavar SG, Singh AD, Shields CL, et al. Postenucleation adjuvant therapy in high-risk retinoblastoma. Arch Ophthalmol 2002; 120(7):923–931.

15. Bosaleh A, Sampor C, Solernou V, et al. Outcome of children with retinoblastoma and isolated choroidal invasion. Arch Ophthalmol 2012;130(6):724–729.

16. Kaliki S, Shields CL, Rojanaporn D, et al. High-risk retinoblastoma based on international classification of retinoblastoma: analysis of 519 enucleated eyes. Ophthalmology 2013;120(5):997–1003.

17. Khelfaoui F, Validire P, Auperin A, et al. Histopathologic risk factors in retinoblastoma: a retrospective study of 172 patients treated in a single institution. Cancer 1996; 77(6):1206–1213.

18. Linn Murphree A. Intraocular retinoblastoma: the case for a new group classification. Ophthalmol Clin North Am 2005;18(1):41–53, viii.

19. Shields CL, Mashayekhi A, Au AK, et al. The International Classification of Retinoblastoma predicts chemoreduction success. Ophthalmology 2006;113(12):2276–2280.

20. Shields CL, Fulco EM, Arias JD, et al. Retinoblastoma frontiers with intravenous, intra-arterial, periocular, and intravitreal chemotherapy. Eye (Lond) 2013;27(2):253–264.

21. Yannuzzi NA, Francis JH, Marr BP, et al. Enucleation vs ophthalmic artery chemosurgery for advanced intraocular retinoblastoma: a retrospective analysis. JAMA Ophthalmol 2015;133(9):1062–1066.

22. Suzuki S, Yamane T, Mohri M, Kaneko A. Selective ophthalmic arterial injection therapy for intraocular retinoblastoma: the long-term prognosis. Ophthalmology 2011; 118(10):2081–2087.

23. Ong SJ, Chao AN, Wong HF, Liou KL, Kao LY. Selective ophthalmic arterial injection of melphalan for intraocular retinoblastoma: a 4-year review. Jpn J Ophthalmol 2015;59(2):109–117.

24. Zhao J, Dimaras H, Massey C, et al. Pre-enucleation chemotherapy for eyes severely affected by retinoblastoma masks risk of tumor extension and increases death from metastasis. J Clin Oncol 2011;29(7):845–851.

25. Chantada G, Leal-Leal C, Brisse H, et al. Is it pre-enucleation chemotherapy or delayed enucleation of severely involved eyes with intraocular retinoblastoma that risks extraocular dissemination and death? J Clin Oncol 2011;29(24):3333–3334; author reply 3335–3336.

26. Brisse HJ, de Graaf P, Galluzzi P, et al. Assessment of early-stage optic nerve invasion in retinoblastoma using high-resolution 1.5 Tesla MRI with surface coils: a multicentre, prospective accuracy study with histopathological correlation. Eur Radiol 2015;25(5): 1443–1452.

27. Brisse HJ, Guesmi M, Aerts I, et al. Relevance of CT and MRI in retinoblastoma for the diagnosis of postlaminar invasion with normal-size optic nerve: a retrospective study of 150 patients with histological comparison. Pediatr Radiol 2007;37(7):649–656.

28. Yan J, Zhang H, Li Y. Establishment of the relationship between tumor size and range of histological involvement to evaluate the rationality of current retinoblastoma management. PLoS One 2013;8(11):e80484.

29. de Graaf P, Barkhof F, Moll AC, et al. Retinoblastoma: MR imaging parameters in detection of tumor extent. Radiology 2005;235(1):197–207.

30. Bossuyt PM, Reitsma JB, Bruns DE, et al. The STARD statement for reporting studies of diagnostic accuracy: explanation and elaboration. Ann Intern Med 2003;138(1):W1–W12.

31. Böhning D, Holling H, Patilea V. A limitation of the diagnostic-odds ratio in determining an optimal cut-off value for a continuous diagnostic test. Stat Methods Med Res 2011; 20(5):541–550.

32. Peduzzi P, Concato J, Kemper E, Holford TR, Feinstein AR. A simulation study of the number of events per variable in logistic regression analysis. J Clin Epidemiol 1996; 49(12):1373–1379.

33. Grigorovski N, Lucena E, Mattosinho C, et al. Use of intra-arterial chemotherapy for retinoblastoma: results of a survey. Int J Ophthalmol 2014;7(4):726–730.